

1 On the choice of the optimal frequency analysis of annual extreme rainfall by
2 multifractal approach

3

4 Amanda P. García-Marín^{1,2*}, Renato Morbidelli², Carla Saltalippi², Marco
5 Cifrodelli², Javier Estévez¹ and Alessia Flammini².

6

7 1 Engineering Projects Area, Department of Rural Engineering, University of
8 Cordoba, Spain.

9 2 Department of Civil and Environmental Engineering, University of Perugia,
10 Italy

11 * Corresponding author: amanda.garcia@uco.es

12

13 Abstract

14

15 Intensity Duration Frequency (IDF) curves are important tools for hydraulic and
16 hydrologic design. Considering that there are different approaches to obtain the
17 rainfall quantiles on which the IDF curves are based, the availability of a method
18 to evaluate their reliability is of great importance. With this aim, in this work the
19 multifractal properties of hourly rainfall data recorded at 23 rain gauges in the
20 Umbria Region (Italy) have been used to select the most appropriate frequency
21 analysis method of extreme annual rainfall at each location. Three methods
22 have been tested: Local Frequency Analysis (by fitting at each station extreme
23 annual rainfall data of different durations by a probability distribution function),
24 Regional Frequency Analysis approach based on L-Moments and flood index
25 method (considering the extreme annual rainfall data from all the stations), and

26 a variant of the latter method known as In-site Regional Frequency Analysis
27 (based on the consideration of the station as a region). Therefore, quantiles of
28 rainfall for different durations and return periods have been obtained. These
29 quantiles have been fitted to the Montana Intensity-Duration-Frequency (IDF)
30 curve. The scaling properties of rainfall have been obtained through out the
31 empirical moments scaling function $K(q)$. Their comparison with some scaling
32 behavior properties of the IDF curves has let the selection of the most adequate
33 quantile estimation method at each site, being the Regional Frequency Analysis
34 the most appropriate one for 14 out of the 23 sites included in the study.

35

36 Keywords: extreme rainfall, multifractality, frequency analysis methods.

37

38 1. Introduction

39 IDF curves are widely used in water resources management projects (Hajani
40 and Rahman, 2018) to obtain the value of the design storm depth. They are
41 derived by fitting extreme quantiles of rainfall (obtained from frequency analysis
42 methods) by parametric equations characterized by different number of
43 parameters like: the Montana equation widely used in real applications (Di
44 Baldassarre et al., 2006a), the Temez equation proposed by the Spanish Water
45 Authority Centre of Hydrographic Studies-CEDEX (Témez, 1987), the four-
46 parameter IDF function considered by Koutsoyiannis et al. (1998) or the one
47 propose by Chow et al. (1988). All of these equations let to obtain the values of
48 rainfall intensity, i , as a function of the duration, D , return period, T (or
49 frequency), and some fitted parameters.

50 When observed rainfall extremes are available for a certain duration, the design
51 storm value (quantile of rainfall with a certain duration and return period) can be
52 estimated by fitting on such data a suitable extreme probability distribution
53 function (e.g. Di Baldassarre et al., 2006a). For low return periods, short extreme
54 data series are good enough to estimate quantile values, so that a local or at-
55 site frequency analysis is valid. As the return period value increases, the length
56 of the data series needs to enlarge. Long rainfall data series are usually
57 available for daily durations, but not for shorter time periods. In this situation, a
58 Regional Frequency Analysis shows up as a good option in order to increase
59 the amount of available data and also to improve quantile estimates (e.g.
60 Hosking and Wallis, 1997; Yu et al, 2004; García-Marín et al., 2011; Haddad et
61 al, 2011; Du et al, 2014; Liu et al, 2015; Hajani and Rahman, 2018; Moujahid et
62 al., 2018).

63 This approach solves the problem of lack of data in time with the abundance of
64 data in space. The bigger the sample of data fitted by a probability distribution
65 function the higher confidence is on estimated quantile values (specially for low
66 frequencies of occurrence). A region will be composed with data from different
67 sites that share the same probability distribution function.

68 An alternative approach that is called In-site regionalization consists of applying
69 the regionalization technique to a specific station (e.g. De Salas and
70 Fernández, 2007; Ayuso-Muñoz et al, 2015). Even in this case the amount of
71 available data increases (that is the main aim of the Regional Frequency
72 Analysis), but with data recorded in the same station over different durations.
73 The region will be formed by series that are considered to come from similar
74 frequency distribution as in the standard regionalization technique.

75 IDF curves have been widely analyzed all over the world (e. g. Jakob et al.,
76 2007; Xu and Tung, 2009; Lee et al., 2010; Haddad et al., 2011; Dourte et al.,
77 2013; Du et al., 2014) and different approaches belonging to the
78 aforementioned techniques have been adopted to obtain them (Elsebaie, 2011;
79 Mamoon et al., 2014; Liu et al., 2015). Some studies show comparisons
80 between at site and regional estimates. Haddad et al. (2011) found that regional
81 design rainfall estimates were generally greater than the at-site estimates.
82 Moujahid et al., (2018) found an increase in events intensities derived from
83 Regional Frequency Analysis. Hajani and Rahman (2018) compared IDF curves
84 derived by different distributions and methods and found that the regional
85 curves values were generally higher than the at-site IDF ones. Despite the
86 existence of these works, a widely recognized method to evaluate the reliability
87 of different quantile estimate approaches to obtain IDF curves that best
88 reproduces the behavior of real extreme annual rainfall data in a certain place is
89 still lacking.

90 Rainfall and Intensity-Duration-Frequency (IDF) curves satisfy scaling relations
91 that are based on the complexity of rainfall that exhibits self-similarity at
92 different scales and can be considered as fractal (e.g. Schertzer and Lovejoy,
93 1987; de Lima and Grasman, 1999; Kiely and Ivanova, 1999; Castro et
94 al.,2004; Langousis et al., 2009; García-Marín et al., 2013; Valencia et al.,
95 2010; Schertzer and Lovejoy, 2011; Rodríguez et al., 2013; Casas-Castillo et
96 al., 2018). Self-similarity processes look the same regardless of the scale where
97 they are observed. Fractal processes exhibit the same behavior for different
98 scale measurements, so they are self-similar. Fractal self-similarity of rainfall
99 has a statistical nature so that its scaling properties can be expressed by

100 statistical relationships (Schertzer and Lovejoy, 1987; Schertzer and Lovejoy,
101 2011). Moreover, the probability distribution of the annual maximum rainfall
102 intensities follows scale-relationships (Burlando and Rosso, 1996).

103 The scale invariance character of rainfall must be reproduced by any rainfall
104 model. A relation between rainfall fractal behavior and IDF scaling exists as
105 detailed in section 3.4 (e.g. Veneziano and Furcolo, 2002; García-Marín et al.,
106 2013). Specifically, IDF values are simple scaled with a power law dependence
107 on the duration (D) and return period (T). The power law exponent can be
108 calculated from the moment scaling exponent function $K(q)$ that characterizes
109 the multifractality of rainfall time series (Veneziano and Furcolo, 2009).

110 As a novelty and based on the evidence that IDF models satisfy the scaling
111 behavior of rainfall (e.g. Yu et al., 2004; Ghanmi et al, 2016; Rodríguez-Solá et
112 al., 2017; Choi et al., 2018), the objective of this work is to use the multifractal
113 analysis to select the most appropriate frequency analysis method to obtain
114 rainfall quantiles at a certain place. With this purpose the multifractal
115 characterization of hourly rainfall data series in 23 rain gauges stations in the
116 Umbria Region (Italy) is performed. Afterwards, rainfall quantiles are obtained at
117 each place by applying three different methods: Local, Regional and In-site
118 Regional Frequency Analysis. The local or at site rainfall frequency analysis is
119 applied by fitting extreme annual rainfall data registered at each station by the
120 General Extreme Values (GEV) probability distribution function. The regional
121 and In-site regional analysis performed are based on the regionalization
122 methodology proposed by Hosking and Wallis (1997). For the former, the
123 extreme annual rainfall annual data of several durations from all the available
124 stations are used and regionalization is studied for each duration. For the latter,

125 the regionalization is made for each site considering only its extreme annual
126 rainfall data for the available durations. For each frequency analysis method, all
127 the quantiles obtained are fitted by the Montana IDF model. The existing
128 relation between the multifractality of rainfall data previously studied and the
129 scale invariance of the IDF curves is finally used to select the most appropriate
130 rainfall frequency analysis methodology at each place.

131

132 2. Study area and data source

133 In this study, rainfall data from the Umbria Region (central Italy) are used. The
134 Umbria Region, with an extension of 8,456 Km², exhibits a mountainous
135 landscape along its eastern side where Apennine Mountains reach up to 2,000
136 m.a.s.l, and a hilly morphology in the central and western zones with altitudes
137 ranging from 100 to 800 m a.s.l. A wide part of the study area is included in the
138 Tiber River basin, which crosses the Region from North to South-West.

139 Mean annual rainfall for the last century is about 900 mm, with values varying in
140 space from 650 mm to 1450 mm. Based on 1921– 2015 period and a network of
141 more than 90 rain gauges, the highest rainfall values usually take place during
142 the autumn-winter seasons. The highest monthly rainfall values generally occur
143 during the autumn-winter period, together with floods caused by widespread
144 rainfall. The highest and lowest rainfall depths typically take place in November
145 and July, respectively.

146 Over the past 15 years the region has been affected by five significant droughts
147 (2001 to 2003, then in 2007, 2012, 2015 and 2017) as well as by six dangerous
148 flood events (one occurred in 2005, one in 2008, one in 2010, two in 2012 and
149 one in 2013) with very large impacts in economic terms (Morbidelli et al., 2018).

150 The study area is currently monitored through a dense rain gauge network
151 (about 1 rain gauge every 90 Km²) (Figure 1). In this study 23 rain gauge
152 stations characterized by continuous hourly rainfall data from 1992 to 2015 are
153 considered (Table 1 and Figure 1). One of the interests of the multifractal
154 approaches is to use all the available data to extract the best information
155 possible of the process under analysis. Therefore, for the multifractal approach,
156 the continuous hourly rainfall data series are used, whereas for the quantile
157 estimation the extreme annual rainfall data series (composed by the highest
158 rainfall value in a year for a certain duration) are obtained for durations of 1, 3,
159 6, 12 and 24 hours.

160

161 3. Methodology

162 3.1. Multifractality

163 Fractal and multifractal approaches can be used for modelling time series and
164 deriving predictions regarding extreme events. Multifractal analysis is applicable
165 to variables self-similarly distributed on a geometric support that is represented
166 by a line (i.e., time series), plane, volume, or fractal set. To identify
167 multifractality in hydrological time series it can be assumed that the variability of
168 the process under study can be modeled as a stochastic turbulent cascade
169 process (Shertzer and Lovejoy , 1987; Gupta and Waymare, 1993; Over and
170 Gupta, 1994; Lovejoy and Schertzer, 1995). A cascade process can be
171 described as eddies breaking up into smaller sub-eddies, each of which
172 receives a part of the flux from its parent body. This cascade process-type
173 behavior can be used with rainfall data to transfer information from some

174 temporal or spatial scales to another, if scale invariance is previously found in
175 the data set.

176 To identify multifractality in rainfall data sets the statistical moments scaling
177 method has been widely applied (Sivakumar, 2001). To perform the analysis,
178 the time series has to be divided into non-overlapping intervals of a certain time
179 resolution. The ratio of the field maximum scale to this interval is the scale ratio,
180 λ . By this process, the time is scaled so that the duration of the longest period
181 of interest is 1 (De Lima and Grasman, 1999). For a time interval i at the scale
182 ratio λ , the mean rainfall intensity is given by $R(\lambda, i)$. In order to obtain non-
183 dimensional values, the mean rainfall intensity $R(\lambda, i)$ has to be normalized by
184 the so-called joint average of the mean rainfall intensities obtained for $\lambda = 1$ (the
185 average found at the higher resolution), $\langle R(1, i) \rangle$, where $\langle \rangle = \left\{ \frac{1}{N_\lambda} \sum_{j=1}^{\lambda} \right\}$, with N_λ
186 the number of non-overlapping time intervals in which the time series is divided
187 for a certain λ . The non-dimensional mean rainfall intensity for an interval i is
188 then obtained as $\varepsilon(\lambda, i) = R(\lambda, i) / \langle R(1, i) \rangle$. The average q^{th} moments of the
189 rainfall intensities of the process at resolution level λ , $\langle \varepsilon_\lambda^q \rangle$, can then be obtained
190 and their scaling can be described by the $K(q)$ function, that satisfies (Schertzer
191 and Lovejoy, 1987; Lovejoy and Schertzer, 1990):

$$192 \quad \langle \varepsilon_\lambda^q \rangle \approx \lambda^{K(q)} \quad (1)$$

193 The scaling behavior given by equation 1 can be investigated by plotting $\langle \varepsilon_\lambda^q \rangle$ as
194 a function of λ in a log-log plot diagram for several values of q . High and low
195 values of q are related to extreme (very high or very low) values of rainfall. The
196 former are conditioned by the length of data and the latter by the resolution of
197 the pluviograph (commonly 0.1 mm). Therefore, a wide range of q moments

198 values greater and lower 1 is recommended to describe the scale behavior of
199 rainfall in a certain place (e.g. De Lima and Grasman, 1999). The linear fits of
200 the log-log plot of equation 1 let to obtain the complete $K(q)$ function and give
201 information about the temporal scale invariance of the data set.

202 Different shapes of $K(q)$ can be expected for mono and multifractal processes.
203 For the former, $K(q)$ versus q is a straight line, whereas for the latter a convex
204 function appears (e.g. Yu et al., 2014). If $K(q)$ is linear through the origin, the
205 measure is self-similar. The value of $K(0)$ is related to the zeros of the data
206 series and also reflects the codimension of the field > 0 .

207 The codimension function $c(\gamma)$ can describe the probability distribution of the
208 process intensity. It also indicates how the histograms of a variable change with
209 resolution. It can be obtained parametrically as $c(q) = q\gamma(q) - K(q)$, where
210 $\gamma(q) = dK(q)/dq$ (Parisi and Frish, 1985; Veneziano and Furcolo, 2002). The
211 value of γ_{max} , which is the maximum value of the order of singularity γ , can
212 provide information about the rare or extreme events in the data series (e.g.
213 Veneziano and Furcolo, 2002).

214

215 3.2. Frequency analysis of extreme events

216 The main objective of frequency analysis is the estimation of extreme events
217 corresponding to different return periods (quantiles) by using probability
218 distribution functions. For this purpose, maximum annual rainfall data series are
219 used, being composed by the highest annual values of rainfall for certain
220 duration. For annual series, the return period of an event is the reciprocal of the
221 probability of exceedance of that event (Koutsoyiannis et al., 1998; Langousis

222 et al., 2009) and can be also defined as the average time interval between
223 exceedances of a certain value.

224 For small return periods or long historical data series, single-site or Local
225 Frequency Analysis (LFA) of extreme data is enough to obtain quantile values.
226 When dealing with rainfall, quantiles are usually estimated to obtain IDF curves.
227 For this purpose, in many studies GEV probability distribution function and its
228 particular form Gumbel are applied to extreme rainfall (Menabde et al., 1999;
229 Bougadis and Adamowski, 2006; Gubareva and Gartsman, 2010; Ghanmi et
230 al., 2016; Choi et al., 2018). The GEV function is preferred for rainfall data
231 series with high extreme values (e.g. Coles, 2001; Koutsoyiannis, 2004;
232 Russell, 2019).

233 Regardless the probability distribution function used for an at-site frequency
234 analysis, the main limitation of this analysis appears when the objective is to
235 estimate extreme rainfall quantiles for high return periods starting from short-
236 length data series. Being this kind of data the most frequently found all over the
237 world, the Regional Frequency Analysis (RFA) appears then as a useful tool to
238 solve the problem of temporal data scarcity by increasing data through the
239 space (e.g. Rostami, 2013).

240 The RFA methodology used in this work was proposed by Hosking and Wallis
241 (1997) and is based on L-moments and the Flood Index method (Dalrymple,
242 1960). The L-moments introduced by Hosking (1990, 1992) are commonly used
243 in RFA of rainfall data (e.g. Yang et al., 2010; Zakaria and Shabri, 2012;
244 Monjahid et al., 2018). They are linear functions of the probability weighted
245 moments (Greenwood et al., 1979). For a sample size n , the estimator of
246 probability weighted moments is given by $b_r = n^{-1} \binom{n-1}{r}^{-1} \sum_{j=r+1}^n \binom{j-1}{r} x_{j:n}$,

247 being x the variable under analysis. The sample L-moments are obtained as
248 linear combinations of b_r , being $l_1 = b_0$, $l_2 = 2b_1 - b_0$, $l_3 = 6b_2 - 6b_1 + b_0$, $l_4 =$
249 $20b_3 - 30b_2 + 12b_1 - b_0$, among others. The L-moments ratios are given by
250 $t_r = l_r/l_2$ (for $r = 3, 4, \dots$). The value of $t = l_2/l_1$ is known as L-coefficient of
251 variation. Flood index procedures are a convenient way of pooling summary
252 statistics from different data samples. The term "flood index" arose because
253 early applications of the procedure were performed on flood data in hydrology
254 (e.g., Dalrymple, 1960), but the method can be used with any kind of data. The
255 key assumption of a flood index procedure is that a group of sites forms a
256 homogeneous region, that is their data sets are characterized by frequency
257 distributions identical apart from a site-specific scaling factor, called flood index.
258 The RFA is advantageous over at-site analysis if homogeneous regions can be
259 compound with the available data series. A homogeneous region is composed
260 by stations that have identical frequency distributions apart from a site-specific
261 scale factor. The obtaining of homogenous regions is the most critical step in
262 RFA and several methodologies and site-characteristics can be applied to
263 group stations into homogeneous regions (e.g. García-Marín et al., 2011, 2015;
264 Medina-Cobo et al., 2017; Satyanarayana and Srinivas, 2011).

265 In order to easily understand the main steps of RFA, appendix A can be seen.
266 As a first step in RFA, L-moments and their corresponding L-moments ratios (L-
267 coefficient of variation ($t^{(i)}$), L-skewness ($t_3^{(i)}$) and L-kurtosis ($t_4^{(i)}$)) have to be
268 obtained for all the data series (for each site or station, i) used in the analysis
269 (notice that (i) changes to (R) if we refer to the region instead of the site). The
270 three L-moments ratios of a certain site are considered as components of a
271 vector in a three-dimensional space with L-moments ratios as coordinates.

272 Considering that each site is then characterized by a vector, the whole set of
 273 stations forms a cloud of points in that space. Any point far from the center of
 274 that cloud (being a point with average L-moments ratios values as coordinates)
 275 has to be considered as discordant and excluded from the analysis.
 276 Specifically, for each station the discordancy, D_i , with respect to the center can
 277 be determined as (Hosking and Wallis, 1997):

$$278 \quad D_i = \frac{1}{3} N (u_i - \bar{u})^T A^{-1} (u_i - \bar{u}) \quad (2)$$

279 where $u_i = (t^{(i)}, t_3^{(i)}, t_4^{(i)})$, $\bar{u} = N^{-1} \sum_{i=1}^N u_i$, $A = \sum_{i=1}^N (u_i - \bar{u})(u_i - \bar{u})$ and N is the
 280 number of stations. If the obtained D_i value exceeds a critical value that
 281 depends on the number of sites and can be found in Hosking and Wallis, 1997,
 282 the site has to be excluded from the analysis because is discordant. The critical
 283 values of discordancy vary from 1.333 for regions of five sites to 3.000 for
 284 regions of fifteen or more sites (Hosking and Wallis, 1997).

285 In order to test if a group of sites forms a homogeneous region, the
 286 heterogeneity measure H , that compares the between-site variations in sample
 287 L-moments for a group of sites with what would be expected for a
 288 homogeneous region, has to be calculated. For that purpose, it is necessary:

289 - to calculate the weighted standard deviation of at-site sample L-

290 coefficient of variation, V , given by $V = \left\{ \frac{\sum_{i=1}^N n_i (t^{(i)} - t^R)^2}{\sum_{i=1}^N n_i} \right\}^{1/2}$, with $t^R =$

291 $\frac{\sum_{i=1}^N n_i t^{(i)}}{\sum_{i=1}^N n_i}$, n the number of data, and $t^{(i)}$ the L-coefficient of
 292 variation of the station;

293 - to fit a kappa distribution to the regional average L-moments ratios;

- 294 - to simulate a large number, N_{sim} , of realizations of a region with N sites,
 295 each having this kappa distribution as its frequency distribution; the
 296 simulated regions are homogeneous and the sites have the same record
 297 lengths as their real-world counterparts;
 298 - to calculate V for each simulated region;
 299 - to determine the mean, μ_v , and standard deviation, σ_v , of N_{sim} values of V
 300 from the simulations.

301 The heterogeneity measure can finally be obtained as:

$$302 \quad H = \frac{(V - \mu_v)}{\sigma_v} \quad (3)$$

303 The region under consideration is acceptably homogeneous when $H < 1$;
 304 possibly heterogeneous when $1 < H < 2$, and definitely heterogeneous for $H > 2$.

305 Once the homogeneity of a region is checked, the quantiles of the variable
 306 analyzed for several return periods can be obtained. Different probability
 307 distribution functions can be tested in order to select the most appropriate to
 308 describe the region and to obtain the regional growth curve, $q(F)$, where F is the
 309 frequency. In a set of three-parameter candidate distributions, to measure the fit
 310 goodness of each one, the following statistics can be calculated:

$$311 \quad Z^{DIST} = (\tau_4^{DIST} - t_4^R + B_4) / \sigma_4 \quad (4)$$

312 where τ_4^{DIST} is the L-kurtosis coefficient of the three-parameter distribution; t_4^R
 313 the regional average L-kurtosis coefficient; σ_4 the standard deviation of t_4^R which
 314 can be obtained by repeated simulation of a homogeneous region whose sites
 315 have the selected three-parameter frequency distribution and record lengths the
 316 same as those of the observed data; and B_4 is the bias in the regional average

317 L-kurtosis for regions with the same number of sites and the same record
318 lengths as the observed data.

319 The fit of a specific distribution is considered to be adequate if the value of
320 statistics $|Z^{DIST}|$ is below or the same as 1.64 at the significance degree of
321 90%.

322 By applying the flood index method, the quantiles Q_i at a site i can then be
323 obtained by,

$$324 \quad Q_i(F) = \mu_i q(F), i = 1 \dots N \quad (5)$$

325 being μ_i the flood index (average of data at site i).

326 Besides the lack of long data series, in some cases there is a lack of spatial
327 information, so a regular RFA cannot be performed. In this case, the
328 regionalization technique can be applied in a single station (de Salas and
329 Fernández, 2007). The station now becomes the region, and the sites of the
330 region are the available data series of different duration. This method is called
331 the In-site Regional Frequency Analysis (IRFA) and can be applied at any
332 location where rainfall records of around 10 min to 24 h duration are available,
333 allowing the development of robust quantiles estimations (Ayuso-Muñoz et al.,
334 2015). The following steps to be followed are the same as stated before.

335

336 3.3. IDF formulation

337 Regardless of the statistical frequency analysis performed, once the quantiles of
338 rainfall are obtained for different durations, an IDF model can be fitted. The
339 most widely used approach consists of using a parametric model characterized
340 typically from 2 to 4 parameters. As the number of parameters increases, the

341 uncertainty of the estimations is amplified as well (Di Baldassarre et al., 2006a,
342 b).

343 Several IDF equations can be found (e.g. Chow, 1964; Bell, 1969; Chen, 1983;
344 García-Bartual and Schneider, 2001), being the one known as Montana Curve
345 one of the most widely used (Di Baldassarre et al., 2006a):

$$346 \quad i(T, D) = aD^{b-1} \quad (6)$$

347 where a and b are the parameters that depend on the return period.

348 This equation shows some limitations for describing the behavior of short-term
349 storms of less than 1 hour (Di Baldassarre et al., 2006a). Nevertheless,
350 considering that it is widely used in the region of the present study and that the
351 work is focused on durations higher than 1 hour, it has been chosen as IDF
352 model.

353

354 3.4. Fractals and IDF

355 As Veneziano and Furcolo (2002) stated, most of the models of IDF curves
356 belongs to self-similar models that satisfy simple-scaling relations, or
357 asymptotically self-similar models. While the IDF curves satisfy simple scaling
358 relations, temporal rainfall has multifractal scale invariance.

359 In engineering practice, the scaling relations between some IDF models and
360 some multifractal parameters can be relevant. They can be used to obtain
361 probable maximum precipitation estimates (Casas-Castillo et al., 2018), rainfall
362 values of low durations by downscaling (Rodríguez-Solá et al., 2017) or rainfall
363 values in un-gauged sites (Ghanmi et al., 2016).

364 One can consider:

365
$$i(T, D) = D^{-h}i(T, 1)$$

366 (7)

367 being h the self-similarity index, D the duration, $i(T, D)$ the intensity value with
368 probability $1/T$, and T the return period.

369 On the other hand, in approximation and for large T :

370
$$i(T, 1) \propto T^\alpha \tag{8}$$

371 where α is a constant (Bendjoudi et al., 1997; 1999).

372 For any finite range of T and $D \rightarrow 0$, Veneziano and Furcolo (2002) obtained that

373 $h = \gamma_1$ and $\alpha = 1/q_1$, where γ_1 is the value of γ where the codimension function

374 $c(\gamma)$ equals 1 and q_1 is the associated moment order.

375 The scaling of IDF can be then expressed by:

376
$$i(T, D) \propto D^{-\gamma_1} T^{1/q_1} \tag{9}$$

377 The parameters γ_1 and q_1 can be obtained from $K(q)$ function (from the linear

378 behavior of the field for q values greater than a given moment) and be related

379 to the slope of the IDF obtained for a certain location. Thus, for each return

380 period analyzed, the absolute value of the IDF slopes ($|b-1|$, equation (6))

381 should be close to the γ_1 value obtained from the multifractal analysis of rainfall

382 data at the same place. Moreover, the slope of the line obtained from plotting

383 the mean rainfall intensity values of several duration for different return periods

384 should be close to the value $1/q_1$ (García-Marín et al., 2013).

385

386 4. Results and discussion

387 4.1. Mutifractal analysis of hourly rainfall in the Umbria Region

388 To obtain the empirical moments scaling exponent function $K(q)$ for the hourly

389 rainfall data series in the 23 rain gauge stations available (Table 1), the log-log

390 plot of the q^{th} average moments of the rainfall intensity ε_λ against the scale ratio
391 λ has to be obtained at each place. Figure 2 shows this plot for three sites:
392 Casacastalda, San Benedetto Vecchio and San Silvestro. As it can be
393 observed, straight lines appear for moments higher (Figure 2a) and lower
394 (Figure 2b) than 1. These straight lines give information about the scaling
395 behavior of the moments observed in the range from 1 hour to 21 days for the
396 three sites. Similar values have been found by other authors for different
397 locations (e.g. Ladoy et al., 1991, 1993; Fraedrich and Larnder, 1993;
398 Svensson et al., 1996; Tessier et al., 1996; Labat et al., 2002; García-Marín et
399 al., 2013; Rodriguez et al., 2013). The same scale invariance regimens have
400 been found for the hourly rainfall data of the other stations in the Umbria region.
401 The empirical function $K(q)$ has been then obtained for the scale regimen
402 detected and for all the sites. In Figure 3 the function $K(q)$ for the same stations
403 of Figure 2 is shown. In all three cases it shows a convex shape that gives
404 information about the multifractal behavior of hourly rainfall at the Umbria
405 region. Important information for the present work can be obtained from $K(q)$
406 function, like the singularity values γ_1 . The value for this parameter varies from
407 0.7219 for Casacastalda, to 0.7945 for San Benedetto Vecchio, with a value of
408 0.7491 for San Silvestro. Table 2 shows the values of γ_1 obtained from the
409 scaling functions at all the sites analyzed, found to vary from 0.7125 to 0.8242.
410 Similar results have been found by García-Marín et al. (2013) and Rodríguez-
411 Solá et al. (2017) for rainfall data in Spanish stations. The value of moment
412 order q_1 associated to γ_1 is also shown in Table 2 for all the sites, and in Figure
413 3 for the selected stations.

414 4.2. Quantile estimation

415 For the 23 rain gauges, the extreme annual rainfall data series are obtained by
416 selecting the maximum rainfall value of certain duration (for durations of 1, 3, 6,
417 12 and 24 hours) for each year of data. The three different frequency analysis
418 methods described in section 3 have been applied. Firstly, a LFA for each
419 extreme data series at each location. Secondly, a RFA of extreme rainfall data
420 for each duration considering all the sites. And finally, an IRFA at each location.
421 For the local analysis the GEV probability distribution function has been used,
422 obtaining quantiles values of extreme rainfall for return periods of 5, 10, 25, 50,
423 100 and 200 years.

424 For each duration, a RFA has been performed (RFA_{ih} with $i = 1, 3, 6, 12$ and 24
425 hours) obtaining the results summarized in Table 3. As first step, the existence
426 of discordant sites was checked by obtaining the values of D_i (equation 2). For
427 the hourly extreme rainfall Regional Frequency Analysis (RFA_{1h}), only Petrelle
428 station was found discordant, and was taken out of the analysis. Two sites
429 resulted discordant for RFA_{3h} , Compignano and San Biagio della Valle; and two
430 more for the RFA_{12h} , being Narni Scalo and San Benedetto Vecchio. For RFA_{6h}
431 and RFA_{24h} no sites were found to be discordant.

432 The heterogeneity measure of the region compound by the remaining stations
433 was then evaluated with equation 3. The values of H were found lower than one
434 for RFA_{1h} (-0.11), RFA_{3h} (0.90), RFA_{12h} (0.54) and RFA_{24h} (0.97). These results
435 show the homogeneity of the regions constituted by the considered stations for
436 the selected durations. For RFA_{6h} the initial value of H was 1.96, which
437 indicated that the region was probably heterogeneous and so it was divided into
438 sub-regions. Following the methodology proposed by García-Marín et al.
439 (2015), the multifractal characteristics of rainfall data were used to divide the

440 RFA_{6h} region into two regions. With the values of γ_1 and $K(0)$ (Table 2) a K-
441 means cluster analysis was performed and two groups of sites were obtained.
442 Two new Regional Frequency Analyses were done, RFA_{6hA} and RFA_{6hB}. The
443 first group was initially composed by 9 sites, whereas 14 stations formed the
444 second. Petrelle station was discordant again, so finally two groups stayed, one
445 with 8 sites and one with 14 stations (Table 3). Both groups were found to be
446 homogeneous according to the values of H parameter, being -0.23 for RFA_{6hA}
447 and -0.83 for RFA_{6hB}, respectively.

448 Once the homogeneous regions have been compounded, the growth curves
449 are necessary in order to finally obtain the quantiles at all the sites. For this
450 purpose, the goodness of a probability distribution function (pdf) in fitting the
451 regional data has to be studied through the value of Z^{DIST} (equation 4). Five
452 three-parameter probability distribution functions were tested, being the
453 Generalized Logistic (GEN-LOG), Generalized Extreme Value (GEV),
454 Generalized Normal (GEN-NOR), Pearson type III (PT-III) and Generalized
455 Pareto (GEN-PAR).

456 Table 4 shows the values of statistics Z^{DIST} obtained by applying equation 4 for
457 all the homogeneous regions and probability distribution functions. According to
458 these results, the most appropriate function for each region is the one that gives
459 the lowest value of $|Z^{DIST}|$ between 0 and 1.64. Based on that, the GEV pdf is
460 the most appropriate for RFA_{3h}, RFA_{6hA} and RFA_{24h}, the GEN-NOR pdf is the
461 best one for RFA_{6hB} and RFA_{12h}, whereas GEN-LOG is the most suitable for
462 RFA_{1h}. The regional growth curves for each region can then be obtained with
463 the selected probability distribution functions for several return periods (Table
464 5). For each duration, considering the calculated growth curve and the average

465 datum at each site, the quantiles for different return periods were obtained by
466 applying the flood index method (equation 5).

467 The IRFA was then applied at each location, considered as one region and
468 each series of a particular duration (5, 10, 15, 20, 30 and 40 min, 1, 3, 6, 12 and
469 24 h) as one site into the region.

470 As it can be seen in Table 6, for 15 out of 23 In-site regions, all durations (sites)
471 formed a homogeneous region with H values less than 1.00. For the In-site
472 regions Forsivo, Gubbio and La Cima, some sites were found to be discordant
473 and were removed from the analysis: 5' and 24 h in Forsivo, 24 h in Gubbio and
474 5', 10', 15', 20' in La Cima. Once the discordant sites were eliminated, the In-
475 site regions became homogeneous according to the H values (Table 6). In-site
476 regions of Montelovesco and San Biagio della Valle, formed a homogeneous
477 region considering all sites, with H values of -0.57 and -2.07, respectively.
478 Nevertheless, no probability distribution function was found as a good candidate
479 to fit the In-site regional data, according to the values of Z^{DIST} obtained. For
480 Montelovesco two subregions were formed, one for durations less than one
481 hour and another for durations greater than one hour (Table 6). Both of them
482 were homogeneous. Petrelle In-site region was heterogeneous considering all
483 sites, so two subregions were formed, and homogeneity results were obtained
484 (Table 6). For San Biagio della Valle, some sites were removed in order to form
485 a homogeneous region. The final In-site homogeneous region was
486 compounded by 7 sites from 30' to 24 h. Similar situation occurred for San
487 Benedetto Vecchio station, where a final homogeneous region was formed
488 removing some sites (Table 6).

489 The regional growth curves for each In-site region were then obtained with the
490 selected probability distribution functions for several return periods (Table 7). As
491 an example, and in order to compare the different approaches, the local,
492 regional and in-site regional quantiles for 24 hours and 50 years of return period
493 are shown in Figure 4. Notice that the values are missing for Forsivo and
494 Gubbio, where 24 h duration was removed from the In-site Regional Frequency
495 Analysis. As it can be seen in this figure, there is no a general pattern in the
496 values obtained by the different methodologies. For 8 sites out of 23 (34.8%)
497 local quantiles are the highest, for 10 sites out of 23 (43.5%) regional quantiles
498 are the highest, whereas In-site quantiles are the highest only for 4 out of 23
499 sites (17.4%). In any case, the different values of quantiles obtained by the
500 three applied methods provide different IDF curves and different design storm
501 values. Thus, it is important to select the most appropriate IDF curve for each
502 site in order to reproduce adequately the extreme rainfall behavior.

503 4.3. IDF fitting

504 All the quantiles of more than one hour of duration obtained by using LFA, RFA
505 and IRFA have been fitted by the Montana IDF model (equation 7). As an
506 example, Table 8 shows the values of parameters a and b for Casacastalda,
507 San Benedetto Vecchio and San Silvestro. It can be noticed that, for each site
508 and frequency analysis, the parameter b has a constant value for all the return
509 periods. This is because when fitting a different b for each T_i ($i = 5, \dots, 200$
510 years) value, it was observed that, in some cases, $i_{D,T_2} < i_{D,T_1}$, being $T_2 > T_1$. In
511 order to avoid that situation, a constant value of b was obtained as the average
512 of all the b values independently estimated for the different return periods.

513

514

515 4.4. Selection of frequency analysis

516 The scale invariance properties of IDF curves and their relationship with
517 multifractal parameters (e.g. Veneziano and Furcolo, 2002; García-Marín et al.,
518 2013) are used in this work to select the most appropriate frequency analysis at
519 each site of the Umbria region.

520 In this context, for each site, the absolute value of slopes of the estimated IDF
521 lines $Slope_{IDF}$ has to be close to the value obtained for the singularity value γ_1
522 in the multifractal analysis of the hourly rainfall data (Table 2). For
523 Casacastalda, San Benedetto Vecchio and San Silvestro, Figure 5a shows
524 $Slope_{IDF}$ for each approach and the singularity value γ_1 obtained for each
525 location. As it can be checked, for Casacastalda the values obtained for LFA
526 and IRFA are lower than γ_1 (0.7219), being the value for Regional Frequency
527 Analysis very close to the singularity value. For San Benedetto Vecchio station,
528 the closest value to γ_1 (0.7945) is that obtained through LFA, whereas at San
529 Silvestro station the IRFA is the most suitable to reproduce the γ_1 value
530 (0.7491).

531 For the same stations, Figure 5b shows the slope of the fit of the rainfall
532 intensity values averaged over durations for different return periods ($Slope_{ARI}$).
533 The slope value has to be close to the value of $1/q_1$ obtained for each location
534 (Table 2). It can be observed that for Casacastalda the closest value to $1/q_1$
535 (0.2222) is the one obtained with RFA, being the results obtained with LFA and
536 IRFA the worst. In San Benedetto Vecchio station, the best result is obtained
537 with LFA, whereas IRFA is the best to fit $1/q_1$ (0.2667) in San Silvestro station.

538 According to the results described above, the IDF curve obtained with quantiles
539 from RFA is the best for Casacastalda station, the one obtained with Local
540 Frequency Analysis quantiles is the most appropriate for San Benedetto
541 Vecchio station, and the IDF curve obtained with quantiles from IRFA is the best
542 choice for San Silvestro station.

543 For the rest of stations, the $|Slope_{IDF}|$ and the $Slope_{ARI}$ values obtained for the
544 three approaches are shown in Table 9. The values in Table 9 have to be
545 compared to those in Table 2 (γ_1, q_1) in order to select the best IDF curve at
546 each location.

547 To better synthesize the results of Figure 5 and Table 9, the values of $(\gamma_1 -$
548 $Slope_{IDF})^2$ and $|Slope_{ARI} - (1/q_1)|$ have been obtained for each site and frequency
549 analysis and shown in Table 10 (e.g. García-Marín et al., 2013).

550 For each multifractal criterium the green values indicate when the LFA is the
551 best, the red values have the same meaning but for RFA, and the blue ones
552 correspond to the best results for IRFA. Combining both multifractal criteria, a
553 decision can be made and a proper frequency analysis can be selected for
554 each site. The selected frequency analysis at each location is shown in bold.
555 Table 10 shows that only for three sites (Città di Castello, Ripalvella and San
556 Benedetto Vecchio stations) the LFA is the best option. IRFA exhibits to be the
557 best choice only at San Silvestro station. RFA is the most appropriate frequency
558 analysis for 14 out of 23 sites. For the rest of stations (5), very close results
559 have been obtained for all frequency analyses, but no coincidence of the two
560 multifractal criteria has been found.

561

562 5. Conclusions

563 The scaling properties of IDF curves are used in this work to select the proper
564 frequency analysis method to obtain quantiles of rainfall in the Umbria Region
565 (Italy). With this purpose, rainfall data series from 23 rainfall gauges were used.
566 The multifractal properties of hourly rainfall were evaluated by applying the
567 statistical moments scaling method. The empirical function $K(q)$ was obtained at
568 each place, and some important multifractal parameters were identified: γ_1 , q_1
569 and the value of $K(0)$.

570 Three frequency analyses of annual maximum rainfall data for different
571 durations have been considered: local, regional and In-site regional frequency
572 analyses. For the Local Frequency Analysis, the GEV probability distribution
573 function was used, and the local quantiles were obtained. The Regional
574 Frequency Analysis proposed by Hosking and Wallis (1997) was performed for
575 each duration, and homogeneous regions of annual maximum rainfall were
576 composed. Different probability distribution functions were tested at each region
577 in order to obtain the regional growth curves and the corresponding quantiles at
578 each location.

579 The Regional Frequency Analysis was also applied at each station (In-site
580 Regional Frequency Analysis), considering the site as a region and the
581 maximum annual rainfall data series as the sites of the region, and the quantiles
582 were derived. Different quantile values were obtained at each station for the
583 different frequency analyses approaches, with no regular pattern for the highest
584 or lowest values for a certain approach.

585 The rainfall quantiles obtained through the different approaches were fitted by
586 the Montana IDF curve. Then, following the theory proposed by Veneziano and
587 Furcolo (2002), the values of γ_1 were compared with the absolute value of

588 slopes of the different IDF curves, and the values of $1/q_1$ were compared to the
589 slope of mean rainfall intensity versus return period fit. These comparisons
590 between multifractal parameters and IDF properties let to select the most
591 appropriate frequency analysis at each location. The Regional Frequency
592 Analysis gave the best results for the 61% of stations, closely followed by the
593 Local Frequency Analysis that was the best option for the 13% of sites. The In
594 site Regional Frequency Analysis was the most appropriate only in one station,
595 and for five more similar values were obtained with the three frequency analysis
596 approaches.

597 Thus, the analysis of the scaling behavior of rainfall proposed here seems to be
598 a good tool to decide which frequency analysis is adequate at a certain place.
599 Lastly, the scaling behavior of rainfall can be analyzed through data sets with
600 time resolution that can vary from fine (e.g. Veneziano and Furcolo 2002;
601 Rodríguez-Solá et al., 2017) to coarse (e.g. Garcia-Marín et al., 2015; Casas-
602 Castillo et al., 2018). When scale invariance is found in a data set, the
603 downscaling or upscaling of maximum rainfall data can be performed. This last
604 procedure let to obtain both quantiles and IDF relations at places where no fine
605 time resolution data are available. Therefore, different types of quantile
606 estimation can be always obtained and the methodology proposed in this work
607 can be useful to decide among them.

608

609 APPENDIX A

610 Figure A.1 shows a flowchart that can summarize the main steps to be
611 followed in RFA. Let suppose a potential region (REGION 1 in Figure 6)
612 composed by n sites with extreme annual rainfall data series. Calculate the L-

613 moments of the data series. Afterwards, obtain the values of discordancy D_i
614 (from equation 2). Remove from the analysis all the m sites with discordancy
615 values greater than the critical one, and repeat this procedure until no
616 discordant site is found. With all the non-discordant sites, calculate the
617 heterogeneity value (H) by applying equation 3. If H value is greater than one,
618 start the process again subdividing REGION 1 into sub-regions. If the H value is
619 lower than one, the region can be considered as homogeneous and the value of
620 Z^{DIST} for a number of candidate probability distribution functions (p.d.f.) has to
621 be obtained by applying equation 4. If the absolute value of Z^{DIST} is lower than
622 1.64 all the data of REGION 1 can be fitted by a p.d.f. (consider the one with
623 the lowest $|Z^{DIST}|$) and the regional growth curve can be obtained. On the
624 contrary, fit the data through the Wakeby p.d.f. Finally, obtain the quantile
625 values Q_i by applying equation 5.

626

627 AKLOWLEDGEMENTS

628 A.P. García-Marín acknowledges the support from the Spanish Ministry of
629 Science, Innovation and Universities with the project AGL2017-87658-R. She
630 also acknowledges the collaboration and hosting of the University of Perugia
631 and specifically of the Hydrology team of the Department of Civil and
632 Environmental Engineering.

633

634 6. References

635 Ayuso-Muñoz, J. L., García-Marín, A. P., Ayuso-Ruíz P., Estévez, J., Pizarro-
636 Tapia, R., Taguas, E. V., 2015. A More Efficient Rainfall Intensity-Duration-
637 Frequency Relationship by Using an “at-site” Regional Frequency Analysis:

638 Application at Mediterranean Climate Locations. Water Resources
639 Management, DOI 10.1007/s11269-015-0993-z.

640 Bell, F. C., 1969. Generalized rainfall-duration-frequency relationships. Journal
641 of Hydraulics Engineering 95(HY1): 311–327.

642 Benjoudi, H., Hubert, P., Schertzer, D., Lovejoy, S., 1997. Interpretation multi-
643 fractale des courbes intensité-duree-frequence des precipitations, Geosci.
644 Surface Hydrol. 325, 323–336.

645 Benjoudi, H., Hubert, P., Schertzer, D., Lovejoy, S., 1999. Multifractal
646 explanation of rainfall intensity-duration-frequency curves, paper presented at
647 EGS 24th General Assembly, Eur. Geophys. Soc., The Hague, Nether-
648 lands, 19-23 April.

649 Bougadis, J., Adamowski, K., 2006. Scaling model of a rainfall intensity–
650 duration–frequency relationship. Hydrological Processes, 20, 3747–3757.
651 <https://doi.org/10.1002/hyp.6386>.

652 Burlando, P, Rosso, R., 1996. Scaling and multiscaling models of deph-
653 duration-frequency curves for storm precipitation. J Hydrol 187:45– 64.

654 Casas-Castillo, M.C., Rodríguez-Solá, R., Navarro, X., Russo, B, Lastra, A.,
655 González, P., Redaño, A., 2018. On the consideration of scaling properties of
656 extreme rainfall in Madrid (Spain) for developing a generalized intensity-
657 duration-frequency equation and assessing probable maximum precipitation
658 estimates. Theor Appl Climatol, 131:573–580.

659 Castro, J., Cârsteanu, A., Flores, C. 2004. Intensity-duration-area frequency
660 functions for precipitation in a multifractal framework. Physica A: Statistical
661 Mechanics and its Applications 338(1–2): 206–210.

662 Chen, C., 1983. Rainfall intensity-duration-frequency formulas. Journal of
663 Hydraulics Engineering 109(12): 1603–1621.

664 Choi, J., Lee, O., Jang, J., Jang, S., Kim, S., 2018. Future intensity–depth–
665 frequency curves estimation in Korea under representative con- centration
666 pathway scenarios of Fifth assessment report using scale-invariance method.
667 Int J Climatol. 1–14. <https://doi.org/10.1002/joc.5850>.

668 Chow, V.T., 1964. Handbook of Applied Hydrology. McGraw- Hill: New York.

669 Chow, V.T., Maidment, D.R., Mays, L.W. 1988. Applied Hydrology. McGraw-
670 Hill: New York.

671 Coles, S., 2001. An introduction to statistical modelling of extreme value.
672 Springer, London.

673 Dalrymple, T., 1960. Flood frequency analysis. USGS, Water Supply Paper
674 1543-A.

675 de Lima, M.I.P., Grasman, J. 1999. Multifractal analysis of 15-min and daily
676 rainfall from a semi-arid region in Portugal. Journal of Hydrology 220: 1–11.

677 de Salas, L., Fernández, J.A., 2007. “In-site” regionalization to estimate an
678 intensity-duration-frequency law: a solution to scarce spatial data in Spain.
679 *Hydrol. Process.* **21**, 3507–3513.

680 Di Baldassarre, G., Brath, A., Montanari, A., 2006a. Reliability of different depth-
681 duration-frequency equations for estimating short-duration design storms. Water
682 Resources Research 42: W12501. DOI: 10.1029/ 2006WR004911.

683 Di Baldassarre, G., Castellarin, G.A., Brath, A., 2006b. Relationships between
684 statistics of rainfall extremes and mean annual precipitation: an application for

685 design-storm estimation in northern central Italy. *Hydrology Earth System*
686 *Sciences* 10: 589–601.

687 Dourte, D., Shukla, S., Singh, P., Haman, D., 2013. Rainfall intensity duration
688 frequency relationships for Andhra Pradesh, India: changing rainfall patterns
689 and implications for runoff and groundwater re-charge. *J Hydrol Eng*
690 18(3):324–330.

691 Du, H., Xia, J., Zeng, S., 2014. Regional Frequency Analysis of extreme
692 precipitation and its spatio-temporal characteristics in the Huai River Basin,
693 China. *Nat Hazards* 70:195–215.

694 Elsebaie, I. H., 2011. Developing rainfall intensity duration frequency
695 relationship for two regions in Saudi Arabia. *J King Saud Univ Eng Sci* 24:131–
696 140.

697 Fraedrich, K., Larnder, C., 1993. Scaling regimes of composite rainfall time
698 series. *Tellus Series A-Dynamic Meteorology and Oceanography* 45A: 289–
699 298.

700 García-Bartual, R., Schneider, M., 2001. Estimating maximum expected short-
701 duration rainfall intensities from extreme convective storms. *Physics and*
702 *Chemistry of the Earth B* 26: 675–681.

703 García-Marín, A. P., Estévez, J., Medina-Cobo, M. T., Ayuso-Muñoz, J. L.,
704 2015. Delimiting homogeneous regions using the multifractal properties of
705 validated rainfall data series. *J Hydrol* 529:106–119.

706 García-Marín, A. P., Ayuso-Muñoz, J. L., Taguas-Ruiz, E. V., Estévez, J., 2011.
707 Regional analysis of the annual maximum daily rainfall in the province of

708 Málaga (southern Spain) using the principal component analysis. *Water*
709 *Environ. J.* 25 (4) 522-531.

710 García-Marín, A. P., Ayuso-Muñoz, J. L., Jiménez-Hornero, F. J., Estévez, J.,
711 2013. Selecting the best IDF model by using the multifractal approach. *Hydrol.*
712 *Process.* 27, 433–443.

713 Ghanmi, H., Bargaoui, Z., Mallet, C., 2016. Estimation of intensity–duration–
714 frequency relationships according to the property of scale invariance and
715 regionalization analysis in a Mediterranean coastal area. *Journal of Hydrology*,
716 541, 38–49. <https://doi.org/10.1016/j.jhydrol.2016.07.002>.

717 Greenwood, J.A., Landwehr, J.M., Matalas, N.C., Wallis, J.R., 1979. Probability
718 weighted moments: definition and relation to parameters of several distributions
719 expressible in Inverse form. *Water Resour. Res.* 15, 1049–1054.

720 Gubareva, T.S., Gartsman, B.I., 2010. Estimating distribution parameters of
721 extreme hydrometeorological characteristics by l-moment method. *Water*
722 *Resour.* 37 (4), 437–445. <http://dx.doi.org/10.1134/S0097807810040020>.

723 Haddad, K., Rahman, A., Green, J., Kuczera, J., 2011. Design Rainfall
724 Estimation for Short Storm Durations Using L-Moments and Generalized Least
725 Squares Regression-Application to Australian Data. *International Journal of*
726 *Water Resources and Arid Environments* 1(3): 210-218.

727 Hajani, E., Rahman, A., 2018. Design rainfall estimation: comparison between
728 GEV and LP3 distributions and at-site and regional estimates. *Nat Hazards*
729 93:67–88.

730 Hosking, J. R. M., 1992. Moments or L-moments? An example comparing two
731 measures of distributional shape. *The American Statistician* 46(3):186–189.

732 Hosking, J. R. M., Wallis, J. R., 1997. Regional Frequency Analysis. An
733 Approach Based on L-Moments. Cambridge. Cambridge University Press.

734 Hosking, J. R. M., 1990. L-moments: Analysis and Estimation of Distributions
735 using Linear Combinations of Order Statistics. Journal of the Royal Statistical
736 Society B 52(1): 105–124.

737 Jakob, D., Xuereb, K., Taylor, B., 2007. Revision of design rainfalls over
738 Australia: a pilot study. Aust J Water Resour 11(2):153–159.

739 Kiely, G., Ivanova, K. 1999. Multifractal analysis of hourly precipitation. Physics
740 and Chemistry of the Earth Part B—Hydrology Oceans and Atmosphere **24**:
741 781–786.

742 Koutsoyiannis, D., Kozonis, D., Manetas, A., 1998. A mathematical framework
743 for studying rainfall intensity duration frequency relation-ships. Journal of
744 Hydrology 206: 118–135.

745 Koutsoyiannis, D., 2004. Statistics of extremes and estimation of extreme
746 rainfall: II. Empirical investigation of long rainfall records/Statistiques de valeurs
747 extrêmes et estimation de précipitations extrêmes: II. Recherche empirique sur
748 de longues séries de précipitations. Hydrological Sciences Journal, 49:4, -610,
749 DOI: 10.1623/hysj.49.4.591.54424.

750 Labat, D., Mangin, A., Ababou, R., 2002. Rainfall-runoffs relations for karstic
751 springs: multifractal analyses. Journal of Hydrology 256: 176–195.

752 Ladoy, P., Lovejoy, S., Schertzer, D., 1991. Extreme variability of climatological
753 data: Scaling and intermittency. In Non-linear variability in Geophysics,
754 Schertzer D, Lovejoy S (eds). Kluwer Acad.: Norwell, Mass; 241–250.

755 Ladoy, P., Schmitt, F., Schertzer, D., Lovejoy, S., 1993. The multifractal
756 temporal variability of Nimes rainfall data. *Comptes Rendus de l' Academie des*
757 *Sciences Serie II* 317(6): 775–782.

758 Langousis, A., Veneziano, D., Furcolo, P., Lepore, Ch., 2009. Multifractal
759 rainfall extremes: theoretical analysis and practical estimation. *Chaos, Solitons*
760 *and Fractals* 39: 1182–1194.

761 Lee, C., Kim, T., Chung, G., Choi, M., Yoo, C., 2010. Application of bivariate
762 frequency analysis to the derivation of rainfall frequency curves. *Stoch Env Res*
763 *Risk Assess* 24:389–397.

764 Liu, J., Doan, C., Liong, S., Sanders, R., Dao, A., Fewtrell, T., 2015. Regional
765 Frequency Analysis of extreme rainfall events in Jakarta. *Nat Hazards* 75:1075–
766 1104.

767 Lovejoy, S., Schertzer, D., 1990. Multifractals, universality classes, satellite and
768 radar measurements of clouds and rain. *Journal of Geophysical Research*
769 95(D3): 2021–2034.

770 Mamoon, A., Joergensen, N. E., Rahman, A., Qasem, H., 2014. Derivation of
771 new design rainfall in Qatar using L-moment based index frequency approach.
772 *Int J Sustain Built Environ* 3:111–118.

773 Medina-Cobo, M. T., García-Marín, A. P., Estévez, J., Jiménez-Hornero, F.J.,
774 Ayuso-Muñoz, J.L., 2017. Obtaining Homogeneous Regions by Determining
775 the Generalized Fractal Dimensions of Validated Daily Rainfall Data Sets.
776 *Water Resouces Management*, 31: 2333-2348.

777 Menabde, M., Seed, A., Pegram, G., 1999. A simple scaling model for extreme
778 rainfall. *Water Resources Research*, 35, 335–339.

779 Monjahid, M., Stour, L., Agoumi, A., Saidi, A., 2018. Regional approach for the
780 analysis of annual maximum daily precipitation in northern Morocco. *Weather*
781 *and Climate Extremes*, 21: 43-51.

782 Morbidelli, R., Saltalippi, C., Flammini, A., Corradini, C., Wilkinson, S. M.,
783 Fowler, H. J., 2018. Influence of temporal data aggregation on trend estimation
784 for intense rainfall. *Advances in Water Resources*, 122: 304-316.

785 Moujahid, M., Stour, L., Agoumi, A., Saidi, A., 2018. Regional approach for the
786 analysis of annual maximum daily precipitation T in northern Morocco. *Weather*
787 *and Climate Extremes* 21 (2018) 43–51.

788 Parisi, G., Frish, U., 1985. A multifractal model of intermittency. In: Ghill M,
789 Benzi R, Parisi G, editors. *Turbulence and predictability in geophysical fluid*
790 *dynamics*. North Holland.

791 Rodríguez-Solá, R., Casas-Castillo, M. C., Redaño, A., 2013. Multifractal
792 analysis of the rainfall time distribution on the metropolitan area of Barcelona
793 (Spain). *Meteorology and Atmospheric Physics* 121(3–4): 181–187.

794 Rodríguez-Solá, R., Casas-Castillo, M.C., Navarro, X., Redaño, A., 2017. A
795 study of the scaling properties of rainfall in Spain and its appropriateness to
796 generate intensity–duration–frequency curves from daily records. *International*
797 *Journal of Climatology*, 37, 770–780. <https://doi.org/10.1002/joc.4738>.

798 Rodríguez-Solá, R., Casas-Castillo, M.C., Navarro, X. and Redaño, A., 2017. A
799 study of the scaling properties of rainfall in Spain and its appropriateness to
800 generate intensity–duration–frequency curves from daily records. *International*
801 *Journal of Climatology*, 37, 770–780. <https://doi.org/10.1002/joc.4738>.

802 Rostami, R., 2013. Regional flood frequency analysis based on l-moment
803 approach (case study: west Azarbaijan Basins). *J. Civ. Eng. Urbanism (JCEU)* 3
804 (3), 107–113.

805 Russell, B.T., 2019. Investigating precipitation extremes in South Carolina with
806 focus on state's October 2015 precipitation event. *Journal of Applied Statistics*,
807 46 (2).

808 Satyanarayana, P., Srinivas, V. V., 2011. Regionalization of precipitation in data
809 sparse areas using large scale atmospheric variables - a fuzzy clustering
810 approach. *J Hydrol* 405:462–473.

811 Schertzer, D., Lovejoy, S., 2011. Multifractals, generalized scale invariance and
812 complexity in geophysics. *Int J Bifurcation Chaos* 21(12):3417– 3456.

813 Schertzer, D., Lovejoy, S., 1987. Physical modelling and analysis of rain and
814 clouds by anisotropic scaling multiplicative processes. *Journal of Geophysical*
815 *Research-Atmospheres* 92: 9693–9714.

816 Svensson, C., Olsson, J., Berndtsson, R., 1996. Multifractal properties of daily
817 rainfall in two different climates. *Water Resources Research* 32: 2463–2472.

818 Témez, J.R. 1987. Cálculo hidrometeorológico de caudales máximos en
819 pequeñas cuencas naturales. Dirección general de carreteras. MOPU: Madrid.

820 Tessier, Y., Lovejoy, S., Hubert, P., Schertzer, D., Pecknold, S., 1996.
821 Multifractal analysis and modelling of rainfall and river flows and scaling, causal
822 transfer functions. *Journal of Geophysical Research- Atmospheres* 101: 26427–
823 26440.

824 Valencia, J.L., Tarquis, A.M., Saa, A., Villeta, M., Gascó, J.M. 2015. Spatial
825 Modeling of Rainfall Patterns over the Ebro River Basin Using Multifractality and

826 Non-Parametric Statistical Techniques. Water 7: 6204–6227.
827 DOI:10.3390/w7116204

828 Veneziano, D., Furcolo, P., 2002. Multifractality of rainfall and scaling of
829 intensity-duration-frequency curves. Water Resources Research 38(12). DOI:
830 10.1029/2001WR000372.

831 Veneziano, D., Furcolo, P., 2009. Improved moment scaling estimation for
832 multifractal signals. Nonlin. Processes Geophys., 16, 641–653, 2009.

833 Xu, Y., Tung, Y., 2009. Constrained scaling approach for design rainfall
834 estimation. Stoch Env Res Risk Assess 23:697–705.

835 Yang, T., Shao, Q., Hao, Z-C., Chen, X., Zhang, Z., Xu, C-Y., Sun, L., 2010.
836 Regional Frequency Analysis and spatio-temporal pattern characterization of
837 rainfall extremes in the Pearl River Basin. Journal of Hydrology 380(3–4): 386–
838 405.

839 Yu, P. S., Yang, T. C., Lin, C. S., 2004. Regional rainfall intensity formulas
840 based on scaling property of rainfall. J Hydrol 295(1–4): 108–123.

841 Yu, Z. G., Leung, Y., Chen, Y. D., Zhang, Q., Anh, V., Zhou, Y., 2014.
842 Multifractal analyses of daily rainfall time series in Pearl River basin of China.
843 Physica A, 405: 193-202.

844 Zakaria, Z. A., Shabri, A., 2012. Regional Frequency Analysis of extreme
845 rainfalls using partial L-moments method. Theoretical and Applied Meteorology.
846 DOI: 10.1007/s00704-012-0763-2.

847

848

849 **Figure captions**

850 Figure 1. Rain gauges at the Umbria Region (red triangles). The green squares
851 show the rain gauges used in this work.

852 Figure 2. Log-log plot of the averaged q^{th} moments of the hourly rainfall
853 intensity on the time scales from 1 hour to 21 days, versus the scale ratio λ at
854 Casacastalda, San Benedetto Vecchio and San Silvestro stations. (a) Moments
855 greater than 1; (b) Moments lower than 1. R^2 values higher than 0.9999 for all
856 the fits.

857 Figure 3. Moments scaling exponent function $K(q)$ for the range of scales
858 detected for the averaged q^{th} moments of the hourly rainfall intensity with the
859 value of γ that makes $c(\gamma) = 1$ and the associated moment order q at
860 Casacastalda, San Benedetto Vecchio and San Silvestro stations.

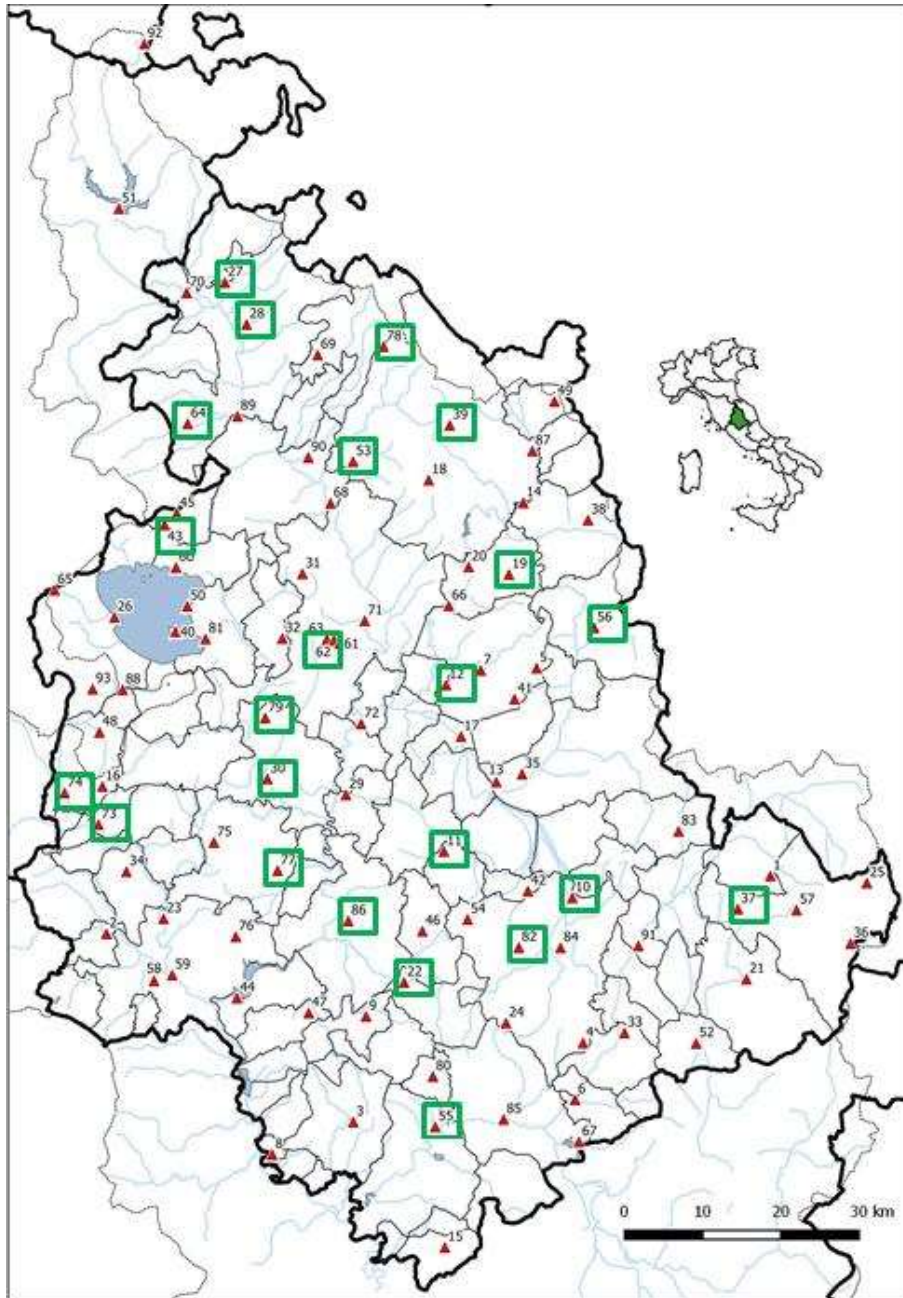
861 Figure 4. Values of the quantiles of 24 hours duration and 50 years of return
862 period obtained by Local, Regional and In-site Regional Frequency Analysis for
863 all the rain gauges used in this work.

864 Figure 5. (a) Comparison between the Slopes_{IDF} (different color symbols for
865 each frequency analysis) and the value of singularity γ_1 , for Casacastalda, San
866 Benedetto Vecchio and San Silvestro stations. (b) For each IDF studied
867 (obtained from Local, Regional o In-site Regional Frequency Analyses
868 quantiles), values of the mean rainfall intensity of all the durations analyzed and
869 for different return periods, at Casacastalda, San Benedetto Vecchio and San
870 Silvestro stations.

871 Figure A.1 Flowchart showing the application steps of the Regional Frequency
872 Analysis.

873

874



875
876

877 Figure 1. Rain gauges at the Umbria Region (red triangles). The green squares
878 show the rain gauges used in this work

879

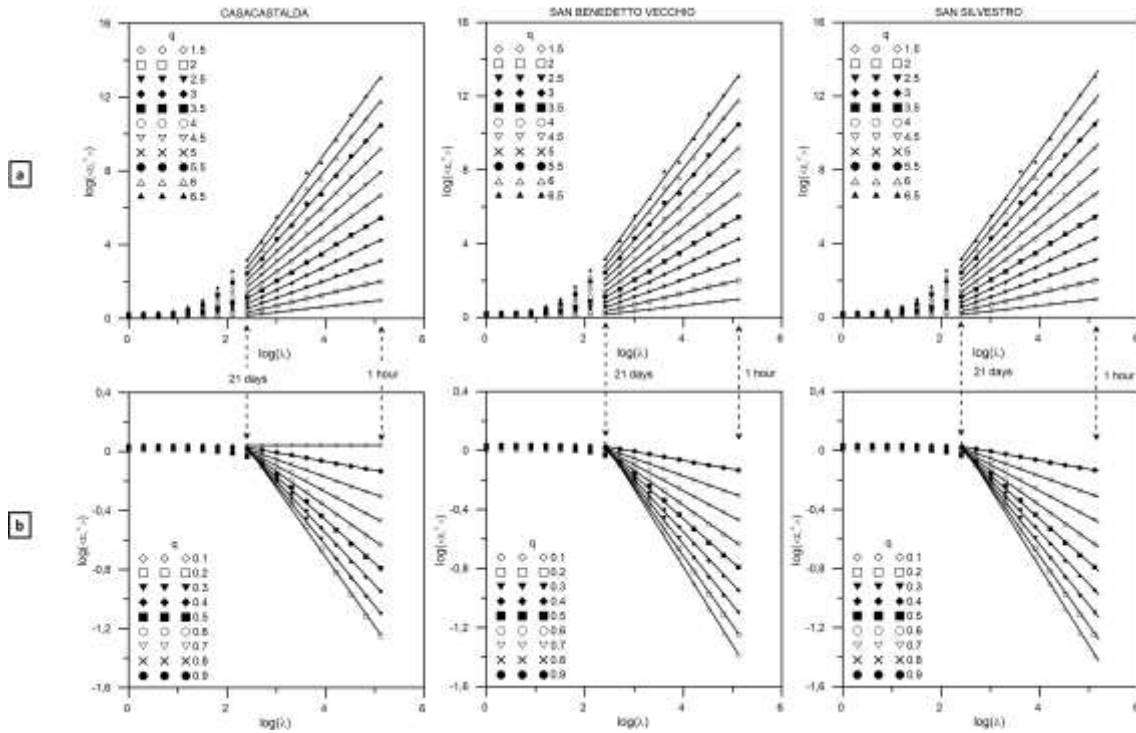
880

881

882

883

884



885

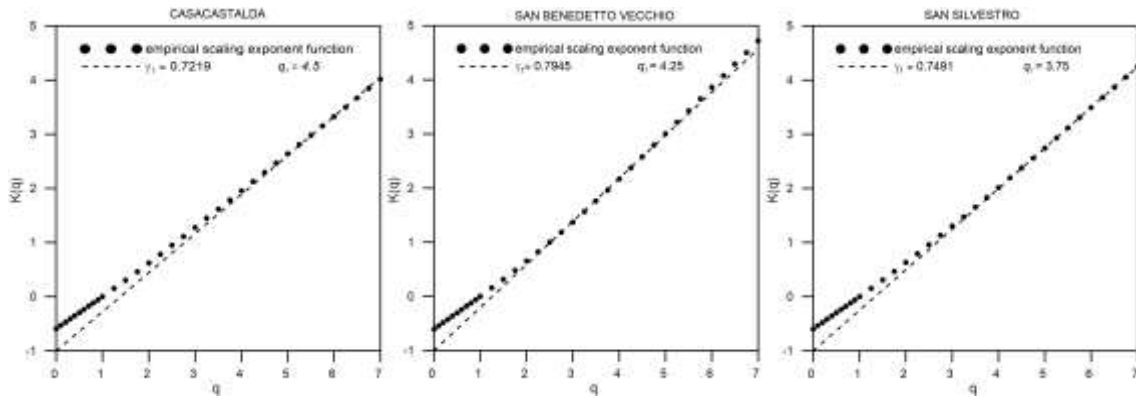
886

887 Figure 2. Log-log plot of the averaged q^{th} moments of the hourly rainfall
 888 intensity on the time scales from 1 hour to 21 days, versus the scale ratio λ at
 889 Casacastalda, San Benedetto Vecchio and San Silvestro stations. (a) Moments
 890 greater than 1; (b) Moments lower than 1. R^2 values higher than 0.9999 for all
 891 the fits.

892

893

894

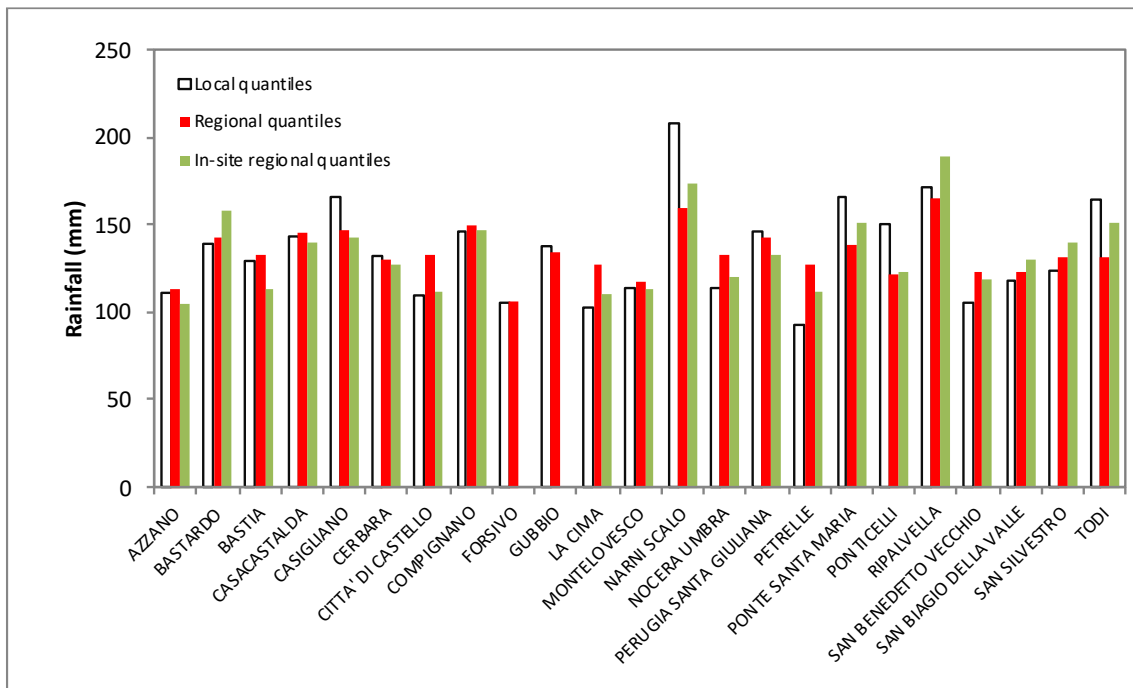


895

896 Figure 3. Moments scaling exponent function $K(q)$ for the range of scales
 897 detected for the averaged q^{th} moments of the hourly rainfall intensity with the
 898 value of γ that makes $c(\gamma) = 1$ and the associated moment order q at
 899 Casacastalda, San Benedetto Vecchio and San Silvestro stations.

900

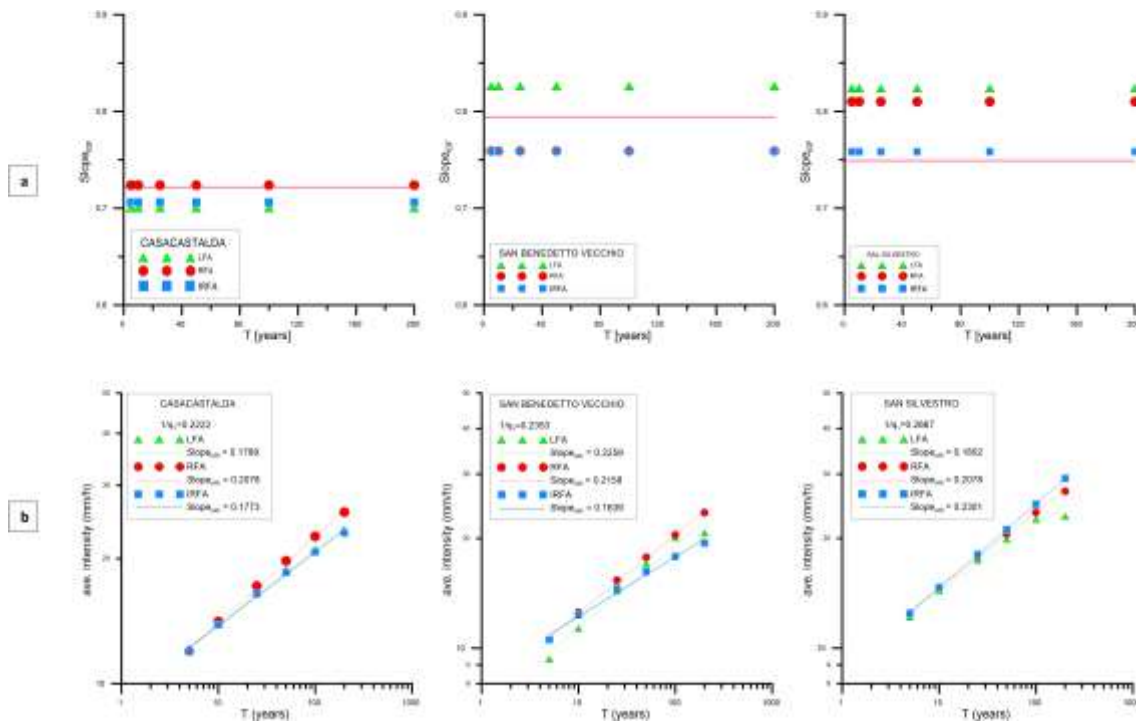
901



902

903 Figure 4. Values of the quantiles of 24 hours duration and 50 years of return
 904 period obtained by Local, Regional and In-site Regional Frequency Analysis for
 905 all the rain gauges used in this work.

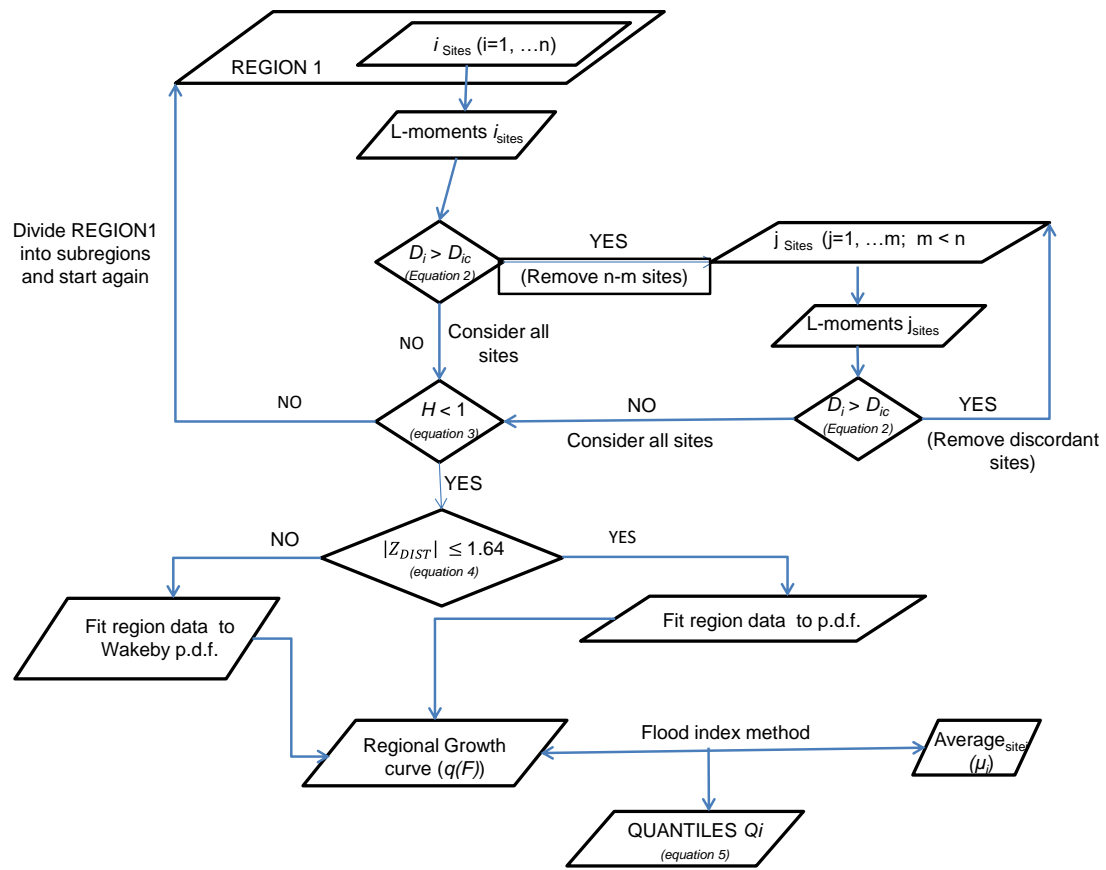
906



907

908 Figure 5. (a) Comparison between the Slopes_{IDF} (different color symbols for
909 each frequency analysis) and the value of singularity γ_1 , for Casacastalda, San
910 Benedetto Vecchio and San Silvestro stations. (b) For each IDF studied
911 (obtained from Local, Regional o In-site Regional Frequency Analyses
912 quantiles), values of the mean rainfall intensity of all the durations analyzed and
913 for different return periods, at Casacastalda, San Benedetto Vecchio and San
914 Silvestro stations.

915



916

917 Figure A.1 Flowchart showing the application steps of the Regional Frequency
918 Analysis.

919

920

921

922

923

924

925

926

927

928 **Table captions**

929 Table 1. Main characteristics of the rain gauges used in this work at the Umbria
930 Region (Italy).

931 Table 2. Values of multifractal parameters obtained from the hourly rainfall data
932 series analyzed. For symbols meaning see the text.

933 Table 3. Heterogeneity results of the Regional Frequency Analysis (RFA)
934 performed for rainfall durations of 1h, 3h, 6h, 12h and 24h at the Umbria region.
935 H is the heterogeneity measure.

936 Table 4. Values of statistics ZDIST for the five probability distribution functions
937 tested at each homogenous region. In red color, the selected probability
938 distribution function according to the value of ZDIST.

939 Table 5. Regional growth curves for different return periods (T) and durations
940 obtained for the homogeneous regions by the selected probability distribution
941 functions.

942 Table 6. In-site Regional Frequency Analysis results for all the stations at the
943 Umbria region. H is the heterogeneity measure, pdf refers to most suitable
944 probability distribution function for the region, and ZDIST is the statistics that
945 measures the goodness of fit.

946 Table 7. In-site Regional Frequency Analysis growth curves for all the sites at
947 the Umbria region and for different return periods (T), obtained from the
948 selected probability distribution functions (details in table 6).

949 Table 8. Values of the IDF parameters, a and b, obtained by fitting the quantiles
950 derived from Local, Regional and In-site Regional Frequency Analyses, for the
951 stations of Casacastalda, San Benedetto Vecchio and San Silvestro.

952 Table 9. Absolute values of slopes of IDF curves slope, SlopeIDF, slopes and
953 slope of average rainfall intensity fit versus return periods, SlopeARI, at each
954 station obtained with the three adopted approaches (Local, Regional and In-site
955 Regional Frequency Analyses).

956 Table 10. Comparison between the multifractal results and the IDF properties
957 for the selection of the proper frequency analysis at each site. Coloured bold
958 values select the best approach, being bold green for Local, bold red for
959 Regional, and bold blue for In-site Regional Analysis.

960

961

962

963

964

965

966

967

968

969

970

971

972

973

974 Table 1. Main characteristics of the rain gauges used in this work at the Umbria
 975 Region (Italy).

RAIN GAUGE STATION	ID	ALTITUDE (m a.s.l.)	UTM33 X (m)	UTM33 Y (m)	MEAN ANNUAL RAINFALL (mm)
AZZANO	10	235	316615	4742431	782.5
BASTARDO	11	331	300489	4748742	803.8
BASTIA UMBRA	12	203	301377	4769716	705.0
CASACASTALDA	19	730	309715	4783398	971.0
CASIGLIANO	22	273	294947	4732331	869.1
CERBARA	27	310	275092	4821081	834.3
CITTÀ DI CASTELLO	28	304	277643	4815738	883.0
COMPIGNANO	30	240	278394	4758593	756.8
FORSIVO	37	963	337588	4740488	867.0
GUBBIO	39	471	302789	4802329	946.5
LA CIMA	43	791	266480	4790970	1097.1
MONTELOVESCO	53	634	290484	4798142	833.0
NARNI SCALO	55	109	298381	4713916	907.5
NOCERA UMBRA	56	534	320281	4776405	937.6
PERUGIA SANTA GIULIANA	62	417	287387	4775762	892.5
PETRELLE	64	342	269830	4803553	897.7
PONTE SANTA MARIA	73	240	256802	4753550	790.1
PONTICELLI	74	245	252657	4757685	754.0
RIPALVELLA	77	453	279329	4746964	879.1
SAN BENEDETTO VECCHIO	78	729	294749	4812427	831.5
SAN BIAGIO DELLA VALLE	79	257	278380	4766281	707.2
SAN SILVESTRO	82	381	309649	4736325	897.9
TODI	86	329	288089	4740319	852.0

976
 977

978

979

980

981

982

983

984

985 Table 2. Values of multifractal parameters obtained from the hourly rainfall data
 986 series analyzed. For symbols meaning see the text.

987

STATION	γ_1	q_1	$K(0)$
AZZANO	0.8029	4.875	-0.6248
BASTARDO	0.7773	5.000	-0.6194
BASTIA UMBRA	0.8052	3.500	-0.6298
CASACASTALDA	0.7219	4.500	-0.5904
CASIGLIANO	0.7905	4.000	-0.6200
CERBARA	0.8052	3.500	-0.6342
CITTÀ DI CASTELLO	0.7406	5.875	-0.6050
COMPIGNANO	0.7881	4.750	-0.6579
FORSIVO	0.8219	4.000	-0.6395
GUBBIO	0.7973	3.750	-0.5932
LA CIMA	0.7838	4.500	-0.5895
MONTELOVESCO	0.7834	5.000	-0.6119
NARNI SCALO	0.7920	4.750	-0.6098
NOCERA UMBRA	0.7125	5.000	-0.5917
PERUGIA SANTA GIULIANA	0.7691	4.875	-0.6043
PETRELLE	0.7311	5.250	-0.6020
PONTE SANTA MARIA	0.8195	3.500	-0.6401
PONTICELLI	0.7659	5.000	-0.6241
RIPALVELLA	0.7759	4.000	-0.6036
SAN BENEDETTO VECCHIO	0.7945	4.250	-0.6091
SAN BIAGIO DELLA VALLE	0.8242	3.500	-0.6389
SAN SILVESTRO	0.7491	3.750	-0.5986
TODI	0.8056	3.500	-0.5899

988

989

990

991

992

993

994

995

996 Table 3. Heterogeneity results of the Regional Frequency Analysis (RFA)
 997 performed for rainfall durations of 1h, 3h, 6h, 12h and 24h at the Umbria region.
 998 H is the heterogeneity measure.

999

RFA _{ih}	Number of stations	Considered stations (ID)	H
RFA _{1h}	22	All except 64	-0.11
RFA _{3h}	21	All except 30 and 79	0.90
RFA _{6h}	23	-	1.96
RFA _{12h}	21	All except 55 and 78	0.54
RFA _{24h}	23	-	0.97
RFA _{6hA}	8	19, 27, 53, 56, 62, 74, 79, 82	-0.23
RFA _{6hB}	14	10, 11, 12, 22, 28, 30, 37, 39, 43, 55, 73, 77, 78, 86	-0.83

1000
 1001
 1002

1003

1004 Table 4. Values of statistics ZDIST for the five probability distribution functions
 1005 tested at each homogenous region. In red color, the selected probability
 1006 distribution function according to the value of ZDIST.

1007
 1008

RFA _{ih}	GEN-LOG	GEV	GEN-NOR	PT-III	GEN-PAR
RFA _{1h}	0.87	-1.04	-1.56	-2.60	-5.45
RFA _{3h}	1.59	-0.25	-0.91	-2.15	-4.63
RFA _{6hA}	1.47	0.03	-0.11	-0.54	-3.08
RFA _{6hB}	2.25	0.76	0.13	-1.01	-2.87
RFA _{12h}	2.54	0.43	-0.02	-0.98	-4.36
RFA _{24h}	1.81	-0.31	-0.81	-1.84	-5.17

1009 GEN-LOG: generalized logistic; GEV: generalized extreme value; GEN-NOR: generalized
 1010 normal; PT-III: Pearson Type

1011

1012

1013 Table 5. Regional growth curves for different return periods (T) and durations
1014 obtained for the homogeneous regions by the selected probability distribution
1015 functions.

	T (years)					
RFA _{ih}	5	10	25	50	100	200
RFA _{1h}	1.23	1.46	1.79	2.07	2.40	2.79
RFA _{3h}	1.24	1.46	1.78	2.02	2.29	2.57
RFA _{6hA}	1.22	1.40	1.63	1.80	1.97	2.14
RFA _{6hB}	1.25	1.49	1.81	2.06	2.33	2.60
RFA _{12h}	1.24	1.45	1.72	1.92	2.12	2.32
RFA _{24h}	1.25	1.47	1.76	1.98	2.21	2.45

1016

1017

1018

1019

1020

1021

1022

1023

1024

1025

1026

1027

1028

1029

1030 Table 6. In-site Regional Frequency Analysis results for all the stations at the
 1031 Umbria region. H is the heterogeneity measure, pdf refers to most suitable
 1032 probability distribution function for the region, and Z^{DIST} is the statistics that
 1033 measures the goodness of fit.

In-site Region	Considered sites	H	pdf	Z^{DIST}
AZZANO	All	-2.08	PT-III	0.62
BASTARDO	All	-1.47	GEV	0.08
BASTIA UMBRA	All	-0.76	GEN-PAR	-1.40
CASACASTALDA	All	-1.14	GEV	0.08
CASIGLIANO	All	-1.23	PT-III	-0.34
CERBARA	All	-1.79	GEN-NOR	-0.29
CITTÀ DI CASTELLO	All	-1.87	PT-III	-0.26
COMPIGNANO	All	-2.59	GEN-NOR	0.16
FORSIVO	All except 5', 24h	-1.04	GEN LOG	0.23
GUBBIO	All except 24 h	0.99	GEN-NOR	0.19
LA CIMA	All except 5', 10', 15', 20'	-0.93	GEN-NOR	-0.02
MONTELOVESCO	1 5', 10', 15', 20', 30', 40'	-0.33	GEN-PAR	-1.17
	2 1, 3, 6, 12, 24 h	0.00	PT-III	0.99
NARNI SCALO	30', 1, 3, 6, 12, 24 h	0.85	PT-III	0.85
NOCERA UMBRA	All	-1.52	PT-III	0.01
PERUGIA SANTA GIULIANA	All	-1.94	GEN-LOG	0.19
PETRELLE	1 5', 10', 15', 20', 12h	0.88	PT-III	1.45
	2 30', 40', 1, 3, 24 h	-0.38	GEN-PAR	1.17
PONTE SANTA MARIA	All	-0.43	GEN-NOR	-0.05
PONTICELLI	All	0.23	PT-III	0.07
RIPALVELLA	All	-1.29	GEN-NOR	0.17
SAN BENEDETTO VECCHIO	30', 1, 3, 6, 12, 24 h	0.99	PT-III	-0.17
SAN BIAGIO DELLA VALLE	30', 40', 1, 3, 6, 12, 24 h	-1.89	GEN-LOG	-1.21
SAN SILVESTRO	All	-1.77	GEN-LOG	-0.11
TODI	All	0.88	GEV	-0.42

1034

1035

1036

1037

1038

1039

1040 Table 7. In-site Regional Frequency Analysis growth curves for all the sites at
 1041 the Umbria region and for different return periods (T), obtained from the
 1042 selected probability distribution functions (details in table 6).

1043

In Site Region	T (years)					
	5	10	25	50	100	200
AZZANO	1.250	1.447	1.584	1.854	2.018	2.177
BASTARDO	1.227	1.475	1.836	2.142	2.482	2.862
BASTIA UMBRA	1.283	1.465	1.635	1.725	1.791	1.840
CASACASTALDA	1.196	1.385	1.644	1.852	2.072	2.306
CASIGLIANO	1.246	1.465	1.739	1.938	2.134	2.325
CERBARA	1.259	1.441	1.658	1.813	1.962	2.107
CITTÀ DI CASTELLO	1.222	1.396	1.607	1.757	1.903	2.044
COMPIGNANO	1.265	1.479	1.747	1.946	2.144	2.344
FORSIVO	1.264	1.498	1.830	2.112	2.427	2.782
GUBBIO	1.246	1.480	1.792	2.036	2.288	2.551
LA CIMA	1.253	1.413	1.596	1.722	1.840	1.953
MONTELOVESCO1	1.316	1.449	1.543	1.580	1.601	1.613
MONTELOVESCO2	1.245	1.425	1.639	1.790	1.934	2.074
NARNI SCALO	1.305	1.613	1.993	2.262	2.515	2.753
NOCERA UMBRA	1.225	1.383	1.568	1.697	1.820	1.937
PERUGIA SANTA GIULIANA	1.213	1.383	1.617	1.807	2.014	2.240
PETRELLE1	1.203	1.345	1.512	1.629	1.740	1.846
PETRELLE2	1.302	1.480	1.638	1.717	1.772	1.811
PONTE SANTA MARIA	1.291	1.542	1.865	2.109	2.357	2.609
PONTICELLI	1.276	1.482	1.729	1.904	2.072	2.234
RIPALVELLA	1.303	1.596	1.988	2.295	2.614	2.947
SAN BENEDETTO VECCHIO	1.232	1.441	1.703	1.894	2.081	2.266
SAN BIAGIO DELLA VALLE	1.213	1.417	1.715	1.974	2.271	2.614
SAN SILVESTRO	1.195	1.408	1.733	2.030	2.382	2.802
TODI	1.234	1.499	1.890	2.228	2.608	3.039

1044
 1045
 1046
 1047
 1048
 1049
 1050
 1051
 1052
 1053
 1054
 1055
 1056
 1057

1058 Table 8. Values of the IDF parameters, *a* and *b*, obtained by fitting the quantiles
 1059 derived from Local, Regional and In-site Regional Frequency Analyses, for the
 1060 stations of Casacastalda, San Benedetto Vecchio and San Silvestro.

STATION	T (years)	IDF-LOCAL		IDF-RFA		IDF-IRFA	
		<i>a</i>	<i>b</i>	<i>a</i>	<i>b</i>	<i>a</i>	<i>b</i>
CASACASTALDA	5	35.54	0.2992	36.55	0.2760	35.53	0.2938
	10	41.19		43.06		41.14	
	25	48.95		52.37		48.83	
	50	55.20		60.25		54.99	
	100	61.84		69.05		61.54	
	200	68.93		78.95		68.50	
SAN BENEDETTO VECCHIO	5	33.40	0.1734	34.05	0.2409	33.96	0.2414
	10	40.52		40.37		39.72	
	25	51.33		49.48		46.94	
	50	60.88		57.23		52.21	
	100	71.89		65.92		57.37	
	200	84.61		75.75		62.46	
SAN SILVESTRO	5	43.34	0.1759	43.50	0.1898	42.25	0.2076
	10	51.22		51.24		49.75	
	25	62.12		62.32		61.27	
	50	70.93		71.70		71.74	
	100	80.36		82.18		84.18	
	200	90.47		93.94		99.06	

1061
 1062
 1063
 1064
 1065

 1066

 1067

 1068

 1069

 1070

 1071

 1072

1073 Table 9. Absolute values of slopes of IDF curves slope, Slope_{IDF}, slopes and
 1074 slope of average rainfall intensity fit versus return periods, Slope_{ARI}, at each
 1075 station obtained with the three adopted approaches (Local, Regional and In-site
 1076 Regional Frequency Analyses).

1077

STATION	Slope _{IDF}			Slope _{ARI}		
	LFA	RFA	IRFA	LFA	RFA	IRFA
AZZANO	0.7492	0.7892	0.7730	0.1543	0.2243	0.1489
BASTARDO	0.7999	0.7673	0.7510	0.2563	0.2161	0.2288
BASTIA UMBRA	0.7276	0.7463	0.7300	0.1829	0.2161	0.0952
CASACASTALDA	0.7007	0.7240	0.7062	0.1789	0.2078	0.1773
CASIGLIANO	0.7046	0.7623	0.7460	0.1795	0.2161	0.1677
CERBARA	0.7363	0.7563	0.7385	0.1819	0.2078	0.1383
CITTÀ DI CASTELLO	0.7095	0.6913	0.7045	0.1590	0.2161	0.1384
COMPIGNANO	0.7272	0.7620	0.7414	0.1336	0.2186	0.1657
FORSIVO	0.8646	0.8373	0.8156	0.2257	0.2200	0.2126
GUBBIO	0.7418	0.7264	0.7030	0.0434	0.2161	0.1932
LA CIMA	0.8111	0.7713	0.8233	0.1398	0.2268	0.1190
MONTELOVESCO	0.7205	0.7697	0.7501	0.1091	0.2077	0.1453
NARNI SCALO	0.6920	0.7556	0.7248	0.2213	0.2158	0.1999
NOCERA UMBRA	0.7265	0.7175	0.6997	0.1320	0.2078	0.1231
PERUGIA SANTA GIULIANA	0.7156	0.7466	0.7288	0.1497	0.2077	0.1655
PETRELLE	0.8239	0.7262	0.7276	0.1534	0.2026	0.0860
PONTE SANTA MARIA	0.7215	0.7469	0.7306	0.2041	0.2161	0.1712
PONTICELLI	0.6425	0.7431	0.7252	0.1280	0.2078	0.1502
RIPALVELLA	0.7395	0.6879	0.6716	0.2498	0.2161	0.2196
SAN BENEDETTO VECCHIO	0.8263	0.7591	0.7586	0.2259	0.2158	0.1639
SAN BIAGIO DELLA VALLE	0.7638	0.7461	0.7139	0.1820	0.2057	0.2072
SAN SILVESTRO	0.8241	0.8102	0.7924	0.1802	0.2078	0.2301
TODI	0.7444	0.7662	0.7499	0.2517	0.2161	0.2434
AZZANO	0.7492	0.7892	0.7730	0.1543	0.2243	0.1489
BASTARDO	0.7999	0.7673	0.7510	0.2563	0.2161	0.2288

1078

1079

1080

1081

1082

1083 Table 10. Comparison between the multifractal results and the IDF properties
 1084 for the selection of the proper frequency analysis at each site. Coloured bold
 1085 values select the best approach, being bold green for Local, bold red for
 1086 Regional, and bold blue for In-site Regional Analysis.

1087

STATION	$(\gamma_1 - Slope_{IDF})^2$			$ Slope_{ARI} - (1/q_1) $		
	LFA	RFA	IRFA	LFA	RFA	IRFA
AZZANO	0.00288	0.00019	0.00089	0.0508	0.0192	0.0562
BASTARDO	0.00051	0.00010	0.00069	0.0563	0.0161	0.0288
BASTIA UMBRA	0.00602	0.00347	0.00566	0.1028	0.0696	0.1905
CASACASTALDA	0.00045	0.00000	0.00025	0.0433	0.0144	0.0449
CASIGLIANO	0.00738	0.00080	0.00198	0.0705	0.0339	0.0823
CERBARA	0.00475	0.00239	0.00445	0.1038	0.0779	0.1474
CITTÀ DI CASTELLO	0.00097	0.00243	0.00130	0.0112	0.0459	0.0318
COMPIGNANO	0.00371	0.00068	0.00218	0.0769	0.0081	0.0448
FORSIVO	0.00182	0.00024	0.00004	0.0243	0.0300	0.0374
GUBBIO	0.00308	0.00503	0.00889	0.2233	0.0506	0.0735
LA CIMA	0.00075	0.00016	0.00156	0.0824	0.0046	0.1032
MONTELOVESCO	0.00396	0.00019	0.00111	0.0909	0.0077	0.0547
NARNI SCALO	0.01000	0.00132	0.00452	0.0108	0.0053	0.0106
NOCERA UMBRA	0.00020	0.00003	0.00016	0.0680	0.0078	0.0769
PERUGIA SANTA GIULIANA	0.00286	0.00051	0.00162	0.0554	0.0026	0.0396
PETRELLE	0.00861	0.00002	0.00001	0.0371	0.0121	0.1045
PONTE SANTA MARIA	0.00960	0.00527	0.00790	0.0816	0.0696	0.1145
PONTICELLI	0.01523	0.00052	0.00166	0.0720	0.0078	0.0498
RIPALVELLA	0.00132	0.00774	0.01088	0.0002	0.0339	0.0304
SAN BENEDETTO VECCHIO	0.00101	0.00125	0.00129	0.0094	0.0195	0.0714
SAN BIAGIO DELLA VALLE	0.00365	0.00610	0.01217	0.1037	0.0800	0.0785
SAN SILVESTRO	0.00563	0.00373	0.00187	0.0865	0.0589	0.0366
TODI	0.00375	0.00155	0.00310	0.0340	0.0696	0.0423

1088

1089

1090